

Dynamics of passing-stars-perturbed binary star systems

D. Bancelin¹★, T. Nordlander^{2,3}, E. Pilat-Lohinger¹ and B. Loibnegger¹

¹*Institute of Astrophysics, University of Vienna, Türkenschanzstrasse 17, A-1180 Vienna, Austria*

²*Division of Astronomy and Space Physics, Department of Physics and Astronomy, Uppsala University, Box 516, 75120 Uppsala, Sweden*

³*Research School of Astronomy and Astrophysics, The Australian National University, Canberra, ACT 2511, Australia*

Accepted XXX. Received YYY; in original form ZZZ

ABSTRACT

In this work, we investigate the dynamical effects of a sequence of close encounters over 200 Myr varying in the interval of 10000 – 100000 au between a binary star system and passing stars with masses ranging from $0.1M_{\odot}$ to $10M_{\odot}$. We focus on binaries consisting of two Sun-like stars with various orbital separations a_0 from 50 au to 200 au initially on circular-planar orbits. We treat the problem statistically since each sequence is cloned 1000 times.

Our study shows that orbits of binaries initially at $a_0 = 50$ au will slightly be perturbed by each close encounter and exhibit a small deviation in eccentricity (+0.03) and in periapsis distance (+1 and -2 au) around the mean value. However increasing a_0 will drastically increase these variances: up to +0.45 in eccentricity and between +63 au and -106 au in periapsis, leading to a higher rate of disrupted binaries up to 50% after the sequence of close encounters. Even though the secondary star can remain bound to the primary, ~20% of the final orbits will have inclinations greater than 10° . As planetary formation already takes place when stars are still members of their birth cluster, we show that the variances in eccentricity and periapsis distance of Jupiter- and Saturn-like planets will inversely decrease with a_0 after successive fly-bys. This leads to higher ejection rate at $a_0 = 50$ au but to a higher extent for Saturn-likes (60%) as those planets' apoapsis distances cross the critical stability distance for such binary separation.

Key words: celestial mechanics – binaries: general – methods: statistical – methods: numerical

1 INTRODUCTION

In our Galaxy, more than 1200 open clusters have been catalogued with masses typically between 10 to $10^4 M_{\odot}$ and a lifetime between some million to billion years (Murdin 2001). Amongst the most famous open clusters, we mention the Pleiades, the nearest star cluster from the Earth which is easily observable by naked eye. It is commonly accepted that stars form in clusters (Lada et al. 1993) and in general they remain part of a cluster for at least 10^8 years (Kroupa 1995, 1998). Therefore, planetary systems or proto-planetary disks will suffer from gravitational perturbations due to stellar encounters in the early stage of a system.

Planetary formation already takes place when stars are still bound to their parent cluster. Indeed, Brucalassi et al. (2014, 2016) identified several hot Jupiters orbiting stars in the dense open cluster M67 and Meibom et al. (2013) reported observations of transits of two G2V stars by planets smaller than Neptune in the billion-year-old NGC6811 open cluster. They concluded that planetary formation is not prohibited in a dense cluster environment as small planets can survive. However, in the early

stage of planetary formation, a planetesimal disk can be severely truncated as shown in Kobayashi & Ida (2001). These authors pointed out that an initial planetesimal disk extending up to 0.8 times the stellar encounter distance (typically 150 – 200 au) and perturbed by passing stars, will lead to a planet-forming region limited to 40 – 60 au, i.e. less than half the initial size of the disk. When giant planets are formed, Spurzem et al. (2009) and de La Fuente Marcos & de La Fuente Marcos (1997) reported that fly-bys can increase the orbital eccentricity and inclination of planets, close encounters that can therefore shrink the size and number of members of planetary systems. According to Fragner & Nelson (2009), close encounters smaller than 150 au, can also significantly increase the mass and semi-major axis of forming giant planets. Laughlin & Adams (1998) pointed out that orbital disruptions can occur when Jovian planets interact with binary stars.

Our Sun is likely to have been formed in a cluster with an initial mass $\geq 500 M_{\odot}$ (Weidner & Kroupa 2004) but dissolved long time ago. However, some siblings of the Sun orbit around the Galactic center at a distance ~ 100 pc from us and could be identified by accurate orbital and physical measurements (Portegies Zwart 2009). The perturbation from close encounters on the dynamical and compositional structure of a protoplanetary disk is such

★ E-mail: david.bancelin@univie.ac.at

that the planetesimal distribution can remain imprinted with this signature over most of the main-sequence lifetime of the star. Indeed, [Ida et al. \(2000\)](#) showed that stellar encounters of pericenter distances between 100 and 200 au could have pumped up the velocity distribution inside Neptune’s 3:2 MMR allowing a more efficient capture of objects into the resonance during a phase of migration of the proto-Neptune. This could explain the high orbital eccentricities and inclinations of the Kuiper Belt objects. In a similar way, [Rickman et al. \(2004\)](#) highlighted also that fly-bys can explain the large periapsis distances observed in the scattered disk. Passing stars can also explain the injection of comets from the Oort cloud into observable orbits i.e. periapsis distances less than 5 au ([Oort 1950](#); [Rickman 1976](#); [Rickman et al. 2005](#); [Fouchard et al. 2007](#)). As shown in [Rickman et al. \(2008\)](#) a huge number of comets from the Oort cloud can enter the observable region within 3 Gyr after the formation of the Sun. Moreover, [Fouchard et al. \(2011\)](#) emphasized the key role of massive stars which can increase the cometary flux by 40%. Recently, [Nordlander et al. \(2017\)](#) investigated the survival of a primordial Oort Cloud, accounting for stellar cluster properties. Independently of the cluster mass, they concluded that an Oort Cloud can survive only when comets orbit at semi-major axes ≤ 3000 au.

Many stars in our galaxy are members of binary systems and most of them must have formed as such ([Goodman & Hut 1993](#)). Effects of an encounter between binary stars (initially at 10 au and on circular orbits) and a passing star have been studied by [Hills \(1975\)](#). They treated the problem statistically considering three family models depending on the mass ratio of the three stars. For each model, the pre-encounter velocity (from 0 – 800 km/s) and impact parameter (0 – 4 times the initial binary separation) were considered as constant. They showed that in addition to changes in the secondary’s orbital elements, close encounters at zero impact parameter (i.e the encounter occurs at the binary’s centre of mass) can either completely break the binary apart or enable the field star to be a stellar member (i.e. one of the original binary components has escaped to infinity). [Heggie & Rasio \(1996\)](#) studied the effect of a fly-by on the secondary star’s eccentricity in clusters assuming the encounter to be both tidal and slow. Their statistical results showed that the change of eccentricity declines in general as a function of a power law of the ratio of the binary’s semi-major axis and the distance of the close encounter.

In our study, we aim to simulate the interactions between a binary star system and a stellar cluster. To this purpose, we investigate the dynamical evolution of binary stars gravitationally perturbed by a sequence of close encounters within 200 Myr. All simulations are performed with respect to the binary centre of mass as we neglect the gravitational perturbation of the cluster field as well as cluster tides. Our approach provides a statistical result as the passing star masses range from $0.1M_{\odot}$ to $10M_{\odot}$ and close encounter distances between 10000 – 100000 au (with respect to the binary centre of mass). Sect. 2 details the fly-by modelling and the numerical integration method of a binary star on the one hand and binary star systems hosting a gas giant planet on the other hand. Then, in Sect. 3, we present our statistical results of the perturbations on binary stars and then on a giant planet initially moving on a circular and planar orbit. Sect. 4 concludes our work.

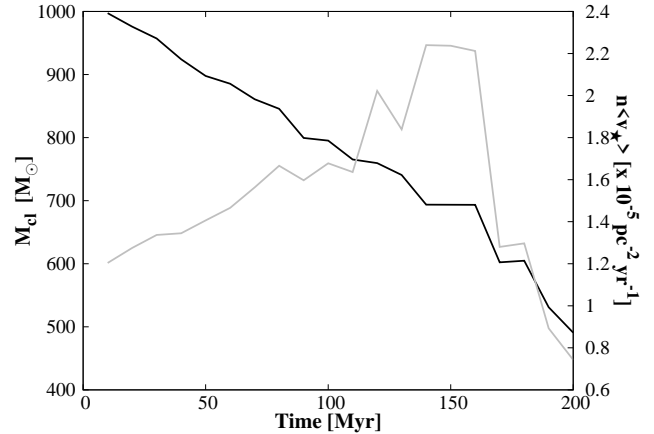


Figure 1. Cluster mass M_{cl} (black) and encounter flux evolution $n < v_{\star} >$ (grey) with time computed at the half-mass radius.

2 METHODS

In this section, we first detail our method for the encounter modelling between a binary star system and interloping stars representing members of a loosely bound cluster. We select the initial mass of this cluster as $M_{cl} = 1000 M_{\odot}$, which is a typical mass of known open clusters ([Murdin 2001](#)). For each computation of a sequence of close encounters, the current mass of the cluster will be taken into account and only the most destructive close encounters will be used to assess the perturbation on the binary star.

2.1 Encounter modelling

To determine an encounter configuration, we proceed with the following 5-steps algorithm:

(1) We pre-compute a sample of encounters relative to the binary barycentre with the corresponding characteristics:

- the mass m_{\star} of the passing star is chosen between $0.1M_{\odot}$ and $10M_{\odot}$ according to the initial stellar mass function as described in [Kroupa \(2001\)](#) with a broken power law function:

$$\Phi(m_{\star}) = \begin{cases} k_1 m_{\star}^{-\alpha_1} & m_0 < m_{\star} \leq m_1 \\ k_2 m_{\star}^{-\alpha_2} & m_1 < m_{\star} \leq m_2 \end{cases} \quad (1)$$

where $\alpha_1 = 1.3$, $\alpha_2 = 2.3$, $m_0 = 0.1M_{\odot}$, $m_1 = 0.5M_{\odot}$ and $m_2 = 150M_{\odot}$. k_1 and k_2 are normalization constants evaluated on the one hand at the limit mass of $\Phi(m_{\star})$ for k_1 and by solving $X_1 + X_2 = 1$ for k_2 on the other hand, with:

$$X_1 = \int_{m_0}^{m_1} \Phi(m_{\star}) dm_{\star} \quad \text{and} \quad X_2 = \int_{m_1}^{m_2} \Phi(m_{\star}) dm_{\star}$$

Finally, the mass m_{\star} is deduced from a random number $\xi \in [0, 1]$ such that:

$$\begin{cases} \text{if } 0 \leq \xi \leq X_1 \text{ then } \int_{m_0}^{m_{\star}} \Phi(m_{\star}) dm_{\star} \Rightarrow m_{\star} \\ \text{if } X_1 \leq \xi \leq X_1 + X_2 \text{ then } X_1 + \int_{m_1}^{m_{\star}} \Phi(m_{\star}) dm_{\star} \Rightarrow m_{\star} \end{cases} \quad (2)$$

As compact remnants such as white dwarfs, neutron stars and black holes likely form with a significant kick that should eject

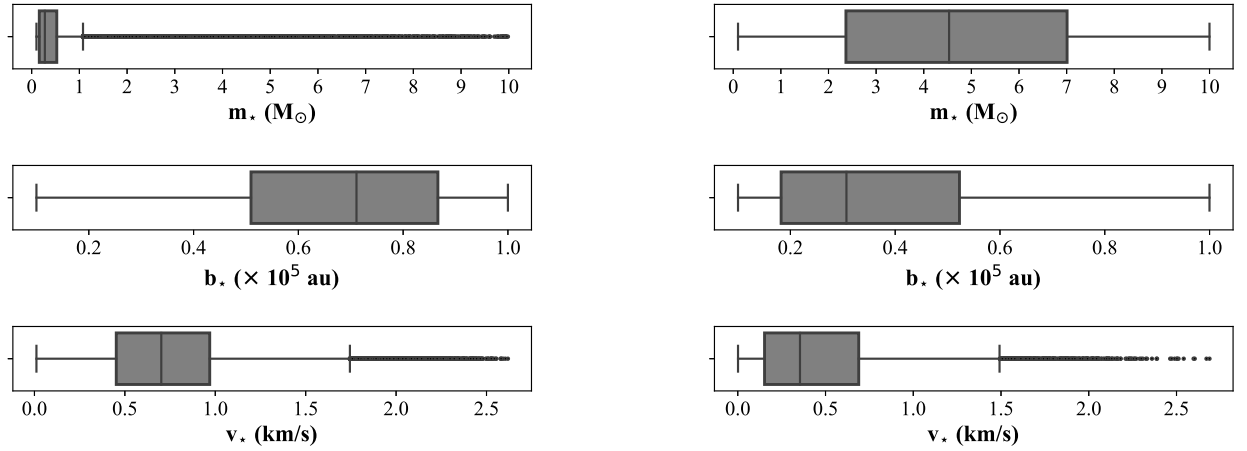


Figure 2. Boxplots showing the distributions in m_* (top), b_* (middle) and v_* (bottom) for the parent distribution of all expected encounters (left) computed from Eqs. (1) – (4), or the most important encounters that are actually executed (right) in Eq. 5. The straight vertical line inside the grey area is for the median value and the outliers are represented by dots outside the edges of the boxplot.

them from a loosely bound cluster, it is unlikely that they would be present in our sample during the timescale of our integration. We therefore identify these cases by evolving each star using the rapid stellar evolution code SSE (Hurley et al. 2000) and only those evolving into one of the three remnant states mentioned above are removed and replaced by another one such that $0.1 M_\odot \leq m_* < 10 M_\odot$.

- we place the star in a cartesian coordinate system \mathbf{d}_* relative to the binary centre such as $|\mathbf{d}_*| = b_*$ where b_* is the impact parameter randomly chosen below $b_{\max} = 100000$ au such that:

$$b_* = \sqrt{\xi} b_{\max} \geq 10000 \text{ au}, \xi \in [0; 1] \quad (4)$$

- we construct \mathbf{d}_* by randomly choosing its longitude $\alpha \in [0 : 2\pi]$ and its latitude δ such that $\sin \delta \in [-1; 1]$.

- to derive the relative velocity v_* with respect to the binary barycentre, we determine the tangential and radial velocity of the barycentre and passing star assuming a flat distribution of angular momentum (King 1966), in a similar way as described in Nordlander et al. (2017).

At the closest approach, the relative velocity \mathbf{v}_* and position \mathbf{d}_* vectors are perpendicular. In order to find the velocity components, we have to solve the following system:

$$\begin{cases} V_x^2 + V_y^2 + V_z^2 = 1 \\ xV_x + yV_y + zV_z = 0 \end{cases} \quad (4)$$

with $V_i = v_i/v_*$ ($i=x,y,z$) and x,y,z being the position coordinates. One can randomly choose one of the three velocity components between $[-1; +1]$ and solve a second order equation to find the two remaining ones.

(2) The first step of the algorithm is iterated until $\sum m_* \geq M_c(t)$ where $M_c(t)$ is the total mass of the cluster according to its age. The evolution and structure of the cluster was computed following Nordlander et al. (2017). Briefly, we used the analytic code EMACSS (Alexander & Gieles 2012; Gieles et al. 2014; Alexander et al. 2014) to compute the evolution of the cluster, and

rescale its lifetime according to the predicted effects of GMC encounters (Gieles et al. 2006). We fit King (1966) models to the predicted mass, half-mass radius and core radius of the cluster every 10 Myr of its evolution. As shown in Fig. 1, the cluster evolves rapidly and loses nearly half of its mass within the 200 Myr period considered here. We also show the expected encounter rate at the half-mass radius, which itself varies with time.

(3) We introduce the parameter S as the approximate impulse which would be transferred to the binary star

$$S = \frac{m_*}{v_* b_*} \quad (5)$$

and we will select among all the pre-computed encounters, the one with the largest S value to account for the single most important encounter.

In Fig. 2 we show the statistics as boxplots of the pre-computed sample of encounters (left) for m_* , b_* and v_* as determined from Eqs. (1) – (4). The extreme borders of these boxplots are for the minimum and maximum values of the data excluding outliers which are represented with dots symbols beyond the maximum value. Inside the grey areas is indicated the median value (vertical line) and their edges represent the 25th and 75th percentiles of the data respectively, meaning that 50% of the pre-computed passing stars will have masses¹ between $0.1 - 0.5 M_\odot$, impact parameters in the range of $0.5 - 0.9 \times 10^5$ au and velocities within $0.5 - 1.0 \text{ km.s}^{-1}$. Maximising the parameter S from Eq. (5) will change the statistics (Fig. 2, right) such that it will instead favour 50% of the values of m_* to lie between $2.5 - 7 M_\odot$, of b_* between $0.2 - 0.5 \times 10^5$ au and of v_* between $0.1 - 0.7 \text{ km.s}^{-1}$.

(4) In order to take into account the whole perturbation of the passing star during its motion, we assume that the star will move on a straight line with a constant velocity \mathbf{v}_* (Rickman et al. 2005; Fouchard et al. 2011) from an initial state \mathbf{d}_*^0 such that $|\mathbf{d}_*^0| = b_{\max}$. The position vector \mathbf{d}_* is thus linearly propagated backwards such

¹ The m_* distribution exhibits many outliers that are overlapping beyond $1 M_\odot$

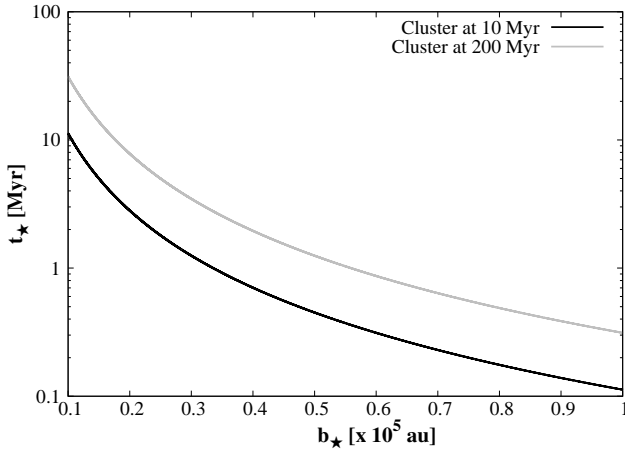


Figure 3. The expected time, on average, between encounters within the impact parameter range b_\star for the cluster at an age of 10 Myr (black) and 200 Myr (grey).

that $\mathbf{d}_\star^0 = \mathbf{d}_\star - \mathbf{v}_\star t_d$ where $t_d = \sqrt{\frac{b_{\max}^2 - b_\star^2}{v_\star^2}}$ is the time needed to reach that position.

(5) Finally, the initial barycentric positions of the primary and secondary components are also propagated to the time before the encounter by the same amount of time t_d .

2.2 Numerical integration of binary star systems

The first part of the simulations consists of integrating the binary star system which is sporadically perturbed by a star in the field. Because of the elliptic motion of a star with respect to the centre of its cluster, the encounter frequency will be highly dependent on its location (Nordlander et al. 2017). As we consider fly-bys with respect to the binary star barycentre we aren't able to account for this dependency. Instead, we follow the approach of Nordlander et al. (2017) by computing the time t_\star separating two encounters according to the impact parameter b_\star . To do so, we took into account a typical value of the encounter flux $n < v_\star >^2$ at the half-mass radius varying with the age of the cluster as shown in Fig. 1 (grey curve). The time between two encounters is deduced from the inverse of the encounter rate, i.e. $t_\star = \frac{1}{nv_\star \pi b_\star}$. As seen in Fig. 3 typical encounters occur more than once per 10 Myr for a cluster of age 10 Myr (black curve) and more than once per 30 Myr for a cluster of age 200 Myr (grey curve). As the selected distribution of b_\star (Fig. 2, right) shows that $\sim 75\%$ of the interactions occur with impact parameters larger than 20 000 au, we therefore select a time between representative encounters $t_\star = 10$ Myr. Fig. 3 clearly indicates that encounters at these distances are likely to occur at least this often. Therefore, one sequence of close encounters every 10 Myr over 200 Myr will contain 20 encounters. This sequence is pre-computed before the simulations by applying the 5-steps algorithm described in Sect. 2.1 every 10 Myr.

We consider the circular-planar case for Sun-analogues binaries with initial separations of $a_0 = 50, 100, 150$ and 200 au. Apart of the mean anomaly of the secondary star randomly chosen

between 0° and 360° , the initial orbital inclination³, argument of periaapsis and longitude of ascending node are all equal to 0° .

We use a semi-analytical method to integrate the motion of a binary star system and the perturbation of passing stars, over 200 Myr in a barycentric frame:

- (i) before and after a close encounter, we use the two-body problem to determine the positions of the stars,
- (ii) during close encounters we use the Lie integrator (Hanslmeier & Dvorak 1984; Bancelin et al. 2012) from the *nine* package (Eggl & Dvorak 2010) to integrate numerically the motion of the three stars. As we want to study the stellar perturbation until the barycentric distance of the passing star theoretically reaches b_{\max} again, we integrate the three bodies over a timescale of $2t_d$ ⁴.

After each encounter, the current orbital parameters of the stellar companion, namely a_b , e_b , i_b and q_b are stored to derive statistical results. Here q_b is the secondary's periaapsis distance.

Finally, for each value a_0 studied we repeat 1000 times the procedure described in Sect. 2.1.

2.3 Perturbations on gas giant planets

In a second step, we investigate the perturbations induced by fly-bys on a gas giant planet initially on a circular-planar orbit at either 5.2 au with a Jupiter mass or at 9.5 au with a Saturn mass. Such initial locations are of interest for planetary formation, since many studies investigated their influences on the dynamical stability of terrestrial planets (Pilat-Lohinger et al. 2008), the water transport from a circumprimary disk of asteroids towards the habitable zone (Bancelin et al. 2016) as well as the location of secular resonances affecting the circumprimary habitable zone of binary star systems (Pilat-Lohinger et al. 2016; Bázso et al. 2017).

The integrations are done separately and differently as we will consider the orbital state of the binary star system after each encounter obtained from the numerical integrations performed in Sect. 2.2 as initial conditions of a three-body problem integrated with the Lie integrator.

3 RESULTS

3.1 Statistical interpretation: I. The intermediate orbit

The statistics on the intermediate orbit i.e. the orbital state before the end of the integration (200 Myr) are made using the so-called quartile parameters commonly used in descriptive statistics. We define the series $\mathbf{P}_x = (a_x, e_x, i_x, q_x)$ constructed according to the orbital state of either the secondary star or a gas giant after each encounter with a passing star over the 1000 clones of sequences of 20 encounters within 200 Myr. We compute the median values $\bar{\mathbf{P}}_x = (\bar{a}_x, \bar{e}_x, \bar{i}_x, \bar{q}_x)$ together with the minimum $\mathbf{P}_{x|\min}$ and maximum $\mathbf{P}_{x|\max}$ absolute deviation from the median value. We use an outliers criteria rejection procedure defined in Tukey (1977) and Frigge et al. (1989) based on the interquartile range I_{QR} parameter which is defined as follows: if $Q_{25}(\mathbf{P}_x)$, $Q_{50}(\mathbf{P}_x)$ and $Q_{75}(\mathbf{P}_x)$ are

³ with respect to the initial orbital plane formed by the binary stars

⁴ Because t_d is defined by the linear motion approximation of the passing star, the latter will actually be located much beyond b_{\max} after the time $2t_d$ due the deviation during an encounter

² $< v_\star >$ represents the average encounter velocities

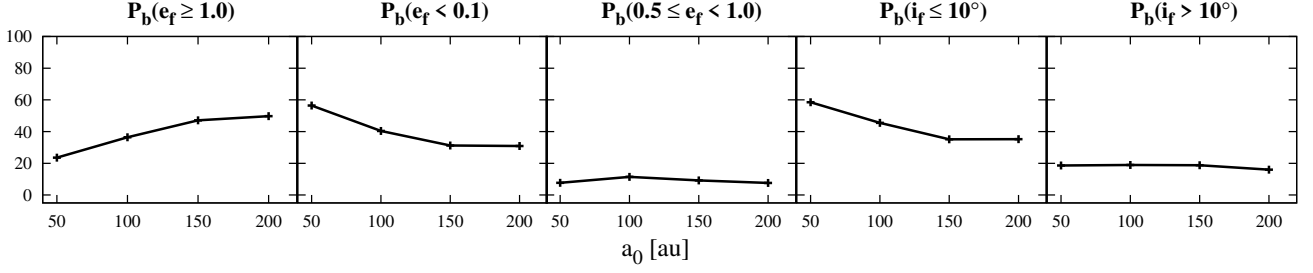


Figure 4. Probability (in percent) of the secondary's final orbit according to its initial location a_0 .

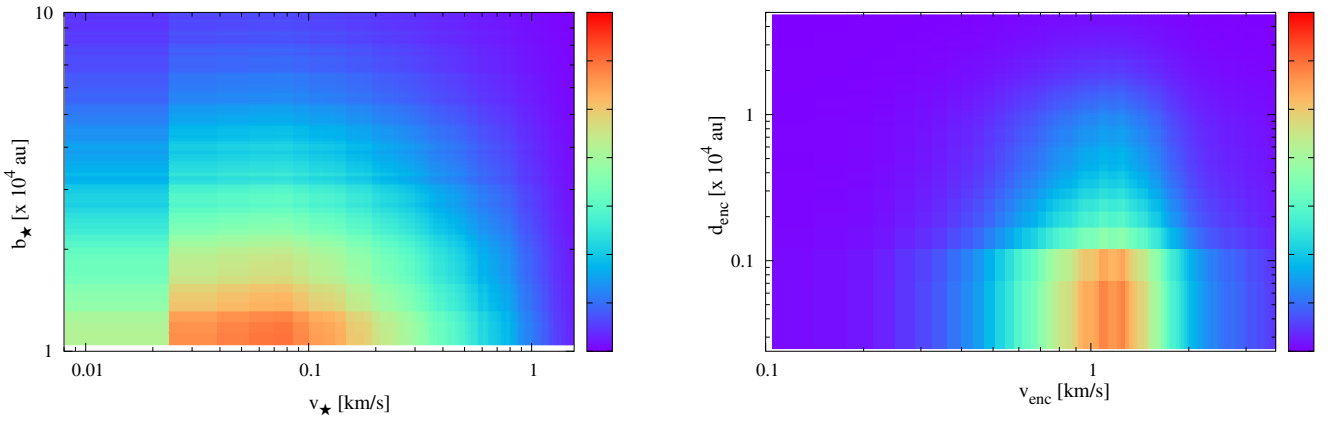


Figure 5. Left: distribution of the 2-body v_* and b_* as selected by the parameter S in Eq. 5. Right: distribution of the encounter velocity and distance v_{enc} and b_{enc} between the passing star and binary's centre in a 3-body configuration.

respectively the 25th, the 50th and the 75th percentiles of the data, Q_{50} being the median value $\bar{\mathbf{P}}_x$, then $I_{QR}(\mathbf{P}_x) = Q_{75}(\mathbf{P}_x) - Q_{25}(\mathbf{P}_x)$. Therefore, a data is defined as an outlier if it lies beyond the interval $[Q_{25}(\mathbf{P}_x) - 1.5 \times I_{QR}(\mathbf{P}_x) : Q_{75}(\mathbf{P}_x) + 1.5 \times I_{QR}(\mathbf{P}_x)]$. After removing the outliers, we compute the minimum and maximum deviations defined as:

$$\begin{aligned} \mathbf{P}_{x[\min]} &= \bar{\mathbf{P}}_x - Q_{25}(\mathbf{P}_x) + 1.5 \times I_{QR}(\mathbf{P}_x) \\ \mathbf{P}_{x[\max]} &= Q_{75}(\mathbf{P}_x) + 1.5 \times I_{QR}(\mathbf{P}_x) - \bar{\mathbf{P}}_x \end{aligned} \quad (6)$$

3.2 Statistical interpretation: II. The final orbit

The statistics on the final orbit are made according to the final orbital elements of the secondary star or a gas giant at the end of the sequence of encounters. Based on their final eccentricity e_f and inclination i_f , we derive the following orbital probabilities defining their final orbit such as:

- (a) hyperbolic i.e. $e_f \geq 1.0$;
- (b) nearly circular i.e. $e_f < 0.1$;
- (c) highly eccentric i.e. $0.5 \leq e_f < 1.0$;
- (d) bound and planar i.e. $e_f < 1.0$ and $i_f \leq 10^\circ$;
- (e) bound and inclined i.e. $e_f < 1.0$ and $i_f > 10^\circ$

3.3 Perturbations on a binary star system

We compile in Tab. 1 the statistical results for the perturbed secondary star – according to its initial separation a_0 – based on the descriptive statistics in Sect. 3.1. The series $\mathbf{P}_b = (a_b, e_b, i_b, q_b)$ is constructed by accounting for the orbital perturbation induced by each stellar encounter before the end of the integration. For each mean value $\bar{a}_b, \bar{e}_b, \bar{i}_b$ and \bar{q}_b we indicate their upper and lower deviations.

One notices that despite the large encounter distances (see Fig. 2), a sequence of fly-bys can significantly modify the initial orbit of the secondary. Although the mean values $(\bar{a}_b, \bar{e}_b, \bar{i}_b, \bar{q}_b) \sim (a_0, e_0, i_0, q_0)$, the upper and lower deviations are significant enough to provoke high perturbations on planetesimal disks. Indeed, $e_{b[\max]}$ can reach +0.04 for $a_0 = 50$ au and +0.45 for $a_0 = 200$ au leading to an initial q_0 reduced by $\sim 4\%$ for $a_0 = 50$ au and by $\sim 54\%$ for $a_0 = 200$ au. Last but not least, variances are large in i_b from $+12^\circ$ for $a_0 = 50$ au to 24° for $a_0 = 200$ au. This is a behaviour predicted by the Gauss perturbation equations as the perturbed inclination of the secondary is $\frac{di_b}{dt} \propto \frac{1}{\sqrt{1-e_b^2}}$ and any increase of e_b due to the passing star will necessarily lead to an increase of i_b .

Figure 4 shows the statistics on the final orbital state of the binary. The middle panel $\mathcal{P}_b(0.5 \leq e_f < 1.0)$ reveals that it is very unlikely that the secondary ends in a highly eccentric orbit and the two possible outcomes are either the binary is dissociated (first panel) or the

Table 1. Statistics on the secondary’s intermediate orbital elements (\bar{a}_b , \bar{e}_b , \bar{i}_b and \bar{q}_b) according to its initial location a_0 . The median value of the distributions are given together with their minimum and maximum deviation (lower and upper script, respectively).

| a_0 [au] | 50 | 100 | 150 | 200 |
|------------------|---------------------------------------|---------------------------------------|--|--|
| \bar{a}_b [au] | 50 ⁺⁰ ₋₀ | 100 ⁺² ₋₄ | 150 ⁺⁵ ₋₈ | 200 ⁺⁷ ₋₁₁ |
| \bar{e}_b | 0.0 ^{+0.04} _{-0.00} | 0.00 ^{+0.36} _{0.00} | 0.00 ^{+0.45} _{-0.00} | 0.00 ^{+0.45} _{-0.00} |
| \bar{i}_b [°] | 0 ⁺¹³ ₋₀ | 1 ⁺²² ₋₁ | 2 ⁺²⁷ ₋₂ | 2 ⁺²⁴ ₋₂ |
| \bar{q}_b [au] | 50 ⁺¹ ₋₂ | 100 ⁺²⁶ ₋₄₄ | 150 ⁺⁵¹ ₋₈₅ | 200 ⁺⁶³ ₋₁₀₆ |

secondary remains in a nearly circular orbit (second panel)⁵. The likelihood of a secondary to remain bound to the primary drops by 20% for $a_0 = 50$ au and by 50% for $a_0 = 200$ au.

Such behaviour is due to the dynamics of the encounter itself. In Fig. 5 we represent a 2-body map of v_\star and b_\star (left) as determined by Eq. 5 where all selected encounters should occur at low relative velocity. This (v_\star, b_\star) distribution corresponds to the linear approximation trajectory of the passing star with respect to the binary’s barycentre. However, because of the mutual perturbation between the binary and the passing star in a 3-body configuration, the encounter distance d_{enc} with the binary centre can be deeper. Therefore, the passing star would fly-by at a higher encounter velocity v_{enc} , as represented on the right side of Fig. 5. As we can see, severe encounters down to $d_{enc} \leq 1000$ au can occur at higher expected velocities in the range $v_{enc} \in [0.5 : 2.0]$ km.s⁻¹. Finally, as predicted by Tab. 1, the very few orbits reaching inclinations beyond 10° will result in lower probabilities for binaries with final inclined orbits (last panel).

3.4 Perturbations on gas giant planets

Figure 6 shows results for the set of orbital elements $\mathbf{P}_p = (a_p, e_p, i_p, q_p)$ for a Jupiter-like (top) and a Saturn-like (bottom) planet where we present the median value $\bar{\mathbf{P}}_p$ (open circle) together with the minimum and maximum values (error bars) of the \mathbf{P}_p series. One important feature exhibited is the variations of both the semi-major axis (first panels) and the eccentricity (second panels) of the planets for tight binary separation. Indeed both gas giants’ initial semi-major axes can drift upwards and downwards by an amount of $\sim 5.2\%$ for Jupiter and $\sim 10\%$ for Saturn. This is due to a dynamical characteristic already mentioned in Bancelin et al. (2016) for binary stars hosting a gas giant planet which can have its initial position periodically shifted by an amount Δa which amplitude depends on the initial periapsis distance q_0 of the secondary star. To highlight this feature, we performed independent simulations in which we varied the initial separation and eccentricity of the binary companion and investigated the perturbations in semi-major axis and eccentricity of a gas giant planet initially on a circular-planar orbit. As seen in the top panel of Fig. 7, the amplitude Δa of a massive planet’s semi-major is stronger for small initial q_0 (top panel).

Another result from these independent simulations shown in Fig. 7 (bottom panel) indicates an increase in eccentricity of the gas giant (also predicted by Georgakarakos (2003)) for decreasing value of q_0 (second panel of the top and bottom figures in Fig. 6).

Especially for a binary’s initial a_0 of 50 au, small changes caused by a fly-by will translate into a change of the parameters for a gas giant orbiting the primary star. As a consequence, a Jupiter’s periapsis distance q_p shows only small variations (Fig. 6, upper figure,

last panel) which moderately perturb embryos, planetary systems or asteroid rings orbiting in lower orbits, whereas a Saturn could nearly destroy any object in that region as its periapsis can reach values down to 6 au.

Finally, the change in orbital inclination of the secondary also translates into a change of the initial orbital inclination of the gas giant and it can be forced to also reach similar maxima as for the binary.

For the final orbital state of a gas giant after a sequence of passing stars, Fig. 8 depicts the orbital outcomes of a Jupiter (black) and a Saturn (blue). Despite the low rate of disrupted binaries at $a_0 = 50$ au as shown in Fig. 4 one can notice that for that binary separation, the rate of ejected Saturns $\mathcal{P}_b(e_f \geq 1.0) \sim 40\%$ is much higher than the rate of ejected Jupiters $\sim 20\%$. This accounts for the critical semi-major axis (Pilat-Lohinger & Dvorak 2002) which added up to its variance (Holman & Wiegert 1999) brings its minimum value down to ~ 12 au for $a_0 = 50$ au. Therefore, Saturn-like planets having apoapsis distances $Q_p \geq 12$ au (Fig. 6) will inevitably be ejected. In spite of the high numbers of ejected binary for $a_0 \geq 100$ au (Fig. 4), giant planets (and therefore a planetary system in the HZ) could survive the loss of a binary companion as we see in Fig. 8 that the rate of ejected gas giants for $a_0 \geq 100$ au doesn’t increase with the rate of disrupted binaries.

If we compare the probabilities $\mathcal{P}_b(0.5 \leq e_f < 1.0)$ and $\mathcal{P}_b(e_f < 0.1)$, one notices that Jupiter- and Saturn-like planets are likely to remain on nearly circular orbits for any value of a_0 except for $a_0 = 50$ au, location of which Saturns will suffer from strong perturbations as mentioned above.

As for the final inclinations (Fig. 8 two last panels), most Jupiters and Saturns still orbiting around the primary despite the fly-bys will end up in orbits with inclinations less than 10° as their plane of orbital motion will be forced to follow the secondary’s change of orbital inclination.

4 CONCLUSIONS

In this paper, we investigated the influence of a sequence of passing stars on the motion of a binary consisting of two G2V stars with various orbital separations and initially moving on circular planar orbits. The sequence of passing stars has been modeled by randomly choosing the mass m_\star , the impact parameter b_\star and velocity v_\star . We treated the problem statistically where we cloned 1000 times a sequence of fly-bys over 200 Myr. A key parameter of the dynamical orbital outcome is the initial separation a_0 of the binary as we showed that placing the secondary further away from the primary will ineluctably lead to a high disruption rate of the system. As gas giant planets can already form while stars are still bound to their birth cluster, we showed that passing stars can indirectly affect the gas giants (e.g. Jupiter- or Saturn-like planets) quite strong through the binary’s perturbed orbit. In our study, we highlighted two possible outcomes according to its initial orbital separation a_0 :

- Either the semi-major axis and eccentricity of the giant planets oscillate after each fly-by – strongly for a Saturn and moderately for a Jupiter – for $a_0 = 50$ au; as a consequence, the rate of ejections of Saturn-like planets is very high ($\sim 40\%$) compared to the Jupiters ($\sim 20\%$);
- or the planet’s semi-major axis and eccentricity remain almost unchanged for $a_0 \geq 100$ au: as a consequence most gas giants will remain on nearly circular orbits.

Important parameters are certainly the periapsis distance and inclination of the gas giant planet. Protoplanetary systems in the re-

⁵ A small fraction of the orbit will have $0.1 \leq e < 0.5$

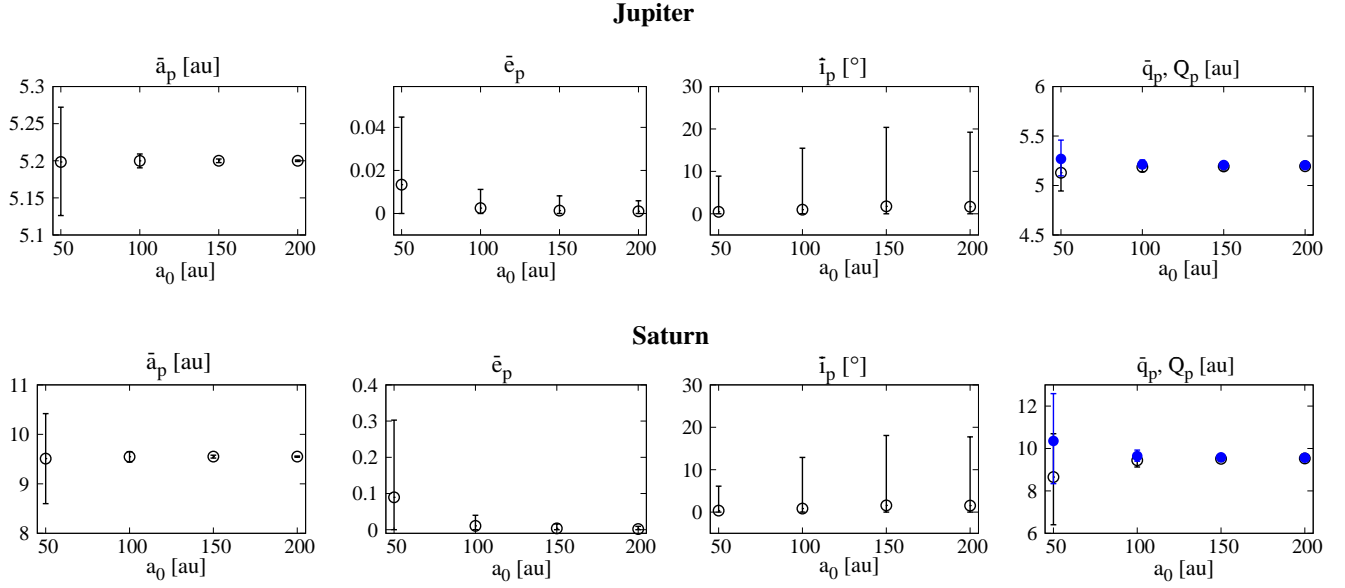


Figure 6. Orbital variations of a Jupiter (top) and a Saturn (bottom) gas giant. The patterns and error bars in blue are for the apoapsis distance of the planet.

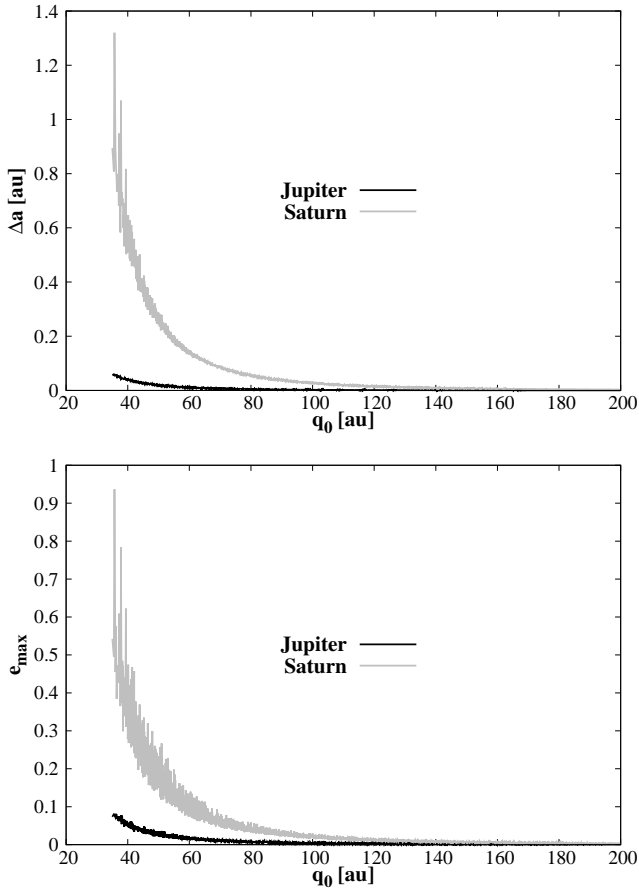


Figure 7. Variations in semi-major axis (top) and maximum eccentricity of a Jupiter (black) and a Saturn (grey) with respect to the initial periapsis q_0 of the secondary star.

gion of the HZ will undoubtedly be indirectly affected by the orbital change of the gas giant caused by fly-bys as shown in [Bitsch et al. \(2013\)](#). For larger initial values of a_0 , a high secondary's inclination might not be critical for planetary formation as shown in [Batygin et al. \(2011\)](#).

An important factor for the habitability of planets formed in the habitable zone is their water content which is strongly correlated to the gas giant and stellar companion's orbital and physical parameters ([Haghighipour & Raymond 2007](#); [Haghighipour et al. 2010](#)) leading to nearly dry planets in the HZ of the host star. However, a circumprimary icy asteroid belt can be the source of water for the entire habitable zone ([Bancelin et al. 2015, 2016](#)) and for embryos or planets up to Earth distances ([Bancelin et al. 2017](#)). In a future work, we aim to study how direct or indirect perturbation from passing stars can influence the water transport to a circumprimary habitable zone from circumstellar or circumbinary disks.

ACKNOWLEDGEMENTS

DB, EPL and BL acknowledge the support of the Austrian Science Foundation (FWF) NFN project: Pathways to Habitability and related sub-projects S11608-N16 "Binary Star Systems and Habitability" and S11603-N16 "Water Transport". DB and EPL acknowledge also the Vienna Scientific Cluster (VSC project 70320) for computational resources.

REFERENCES

- Alexander P. E. R., Gieles M., 2012, MNRAS, 422, 3415
- Alexander P. E. R., Gieles M., Lamers H. J. G. L. M., Baumgardt H., 2014, MNRAS, 442, 1265
- Bancelin D., Hestroffer D., Thuillot W., 2012, Celestial Mechanics and Dynamical Astronomy, 112, 221
- Bancelin D., Pilat-Lohinger E., Eggel S., Maindl T. I., Schäfer C., Speith R., Dvorak R., 2015, A&A, 581, A46
- Bancelin D., Pilat-Lohinger E., Bazsó Á., 2016, A&A, 591, A120

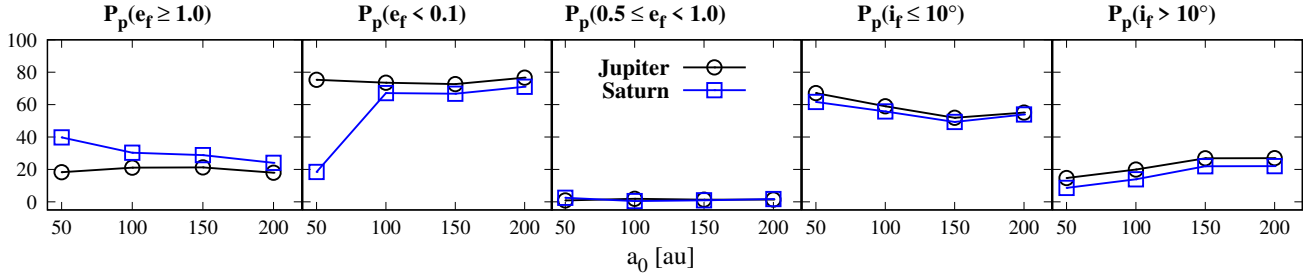


Figure 8. Probability (in percent) of a Jupiter's (black) and a Saturn's (blue) final orbits according to the binary's initial location a_0 .

Bancelin D., Pilat-Lohinger E., Maindl T. I., Ragossnig F., Schäfer C., 2017, *AJ*, 153, 269

Batygin K., Morbidelli A., Tsiganis K., 2011, *A&A*, 533, A7

Bazsó Á., Pilat-Lohinger E., Eggl S., Funk B., Bancelin D., Rau G., 2017, *MNRAS*, 466, 1555

Bitsch B., Crida A., Libert A.-S., Lega E., 2013, *A&A*, 555, A124

Brucalassi A., et al., 2014, *A&A*, 561, L9

Brucalassi A., et al., 2016, *A&A*, 592, L1

Eggl S., Dvorak R., 2010, in Souchay J., Dvorak R., eds, *Lecture Notes in Physics*, Berlin Springer Verlag Vol. 790, *Lecture Notes in Physics*, Berlin Springer Verlag, pp 431–480

Fouchard M., Froeschlé C., Rickman H., Valsecchi G. B., 2007, in Benest D., Froeschlé C., Lega E., eds, *Lecture Notes in Physics*, Berlin Springer Verlag Vol. 729, *Lecture Notes in Physics*, Berlin Springer Verlag, p. 257

Fouchard M., Froeschlé C., Rickman H., Valsecchi G. B., 2011, *Icarus*, 214, 334

Fragner M. M., Nelson R. P., 2009, *A&A*, 505, 873

Frigge M., Hoaglin D. C., Iglewicz B., 1989, *The American Statistician*, 43, 50

Georgakarakos N., 2003, *Monthly Notices of the Royal Astronomical Society*, 345, 340

Gieles M., Portegies Zwart S. F., Baumgardt H., Athanassoula E., Lamers H. J. G. L. M., Sipior M., Leenaarts J., 2006, *MNRAS*, 371, 793

Gieles M., Alexander P. E. R., Lamers H. J. G. L. M., Baumgardt H., 2014, *MNRAS*, 437, 916

Goodman J., Hut P., 1993, *ApJ*, 403, 271

Haghighipour N., Raymond S. N., 2007, *ApJ*, 666, 436

Haghighipour N., Dvorak R., Pilat-Lohinger E., 2010, in Haghighipour N., ed., *Astrophysics and Space Science Library* Vol. 366, *Planets in Binary Star Systems*, p. 285 ([arXiv:0911.0819](https://arxiv.org/abs/0911.0819))

Hanslmeier A., Dvorak R., 1984, *A&A*, 132, 203

Heggie D. C., Rasio F. A., 1996, *MNRAS*, 282, 1064

Hills J. G., 1975, *AJ*, 80, 809

Holman M. J., Wiegert P. A., 1999, *AJ*, 117, 621

Hurley J. R., Pols O. R., Tout C. A., 2000, *MNRAS*, 315, 543

Ida S., Larwood J., Burkert A., 2000, *ApJ*, 528, 351

King I. R., 1966, *AJ*, 71, 64

Kobayashi H., Ida S., 2001, *Icarus*, 153, 416

Kroupa P., 1995, *MNRAS*, 277

Kroupa P., 1998, *MNRAS*, 298, 231

Kroupa P., 2001, *MNRAS*, 322, 231

Lada E. A., Strom K. M., Myers P. C., 1993, in Levy E. H., Lunine J. I., eds, *Protostars and Planets III*, pp 245–277

Laughlin G., Adams F. C., 1998, *ApJ*, 508, L171

Meibom S., et al., 2013, *Nature*, 499, 55

Murdin P., 2001, *Encyclopedia of astronomy and astrophysics*

Nordlander T., Rickman H., Gustafsson B., 2017, *A&A*, 603, A112

Oort J. H., 1950, *Bull. Astron. Inst. Netherlands*, 11, 91

Pilat-Lohinger E., Dvorak R., 2002, *Celestial Mechanics and Dynamical Astronomy*, 82, 143

Pilat-Lohinger E., Süli Á., Robutel P., Freistetter F., 2008, *ApJ*, 681, 1639

Pilat-Lohinger E., Bazsó A., Funk B., 2016, *AJ*, 152, 139

Portegies Zwart S. F., 2009, *ApJ*, 696, L13

Rickman H., 1976, *Bulletin of the Astronomical Institutes of Czechoslovakia*, 27, 92

Rickman H., Froeschlé C., Froeschlé C., Valsecchi G. B., 2004, *A&A*, 428, 673

Rickman H., Fouchard M., Valsecchi G. B., Froeschlé C., 2005, *Earth Moon and Planets*, 97, 411

Rickman H., Fouchard M., Froeschlé C., Valsecchi G. B., 2008, *Celestial Mechanics and Dynamical Astronomy*, 102, 111

Spurzem R., Giersz M., Heggie D. C., Lin D. N. C., 2009, *ApJ*, 697, 458

Tukey J. W., 1977, *Exploratory Data Analysis*, Behavioral Science: Quantitative Methods, Addison-Wesley

Weidner C., Kroupa P., 2004, *MNRAS*, 348, 187

de La Fuente Marcos C., de La Fuente Marcos R., 1997, *A&A*, 326, L21

This paper has been typeset from a \LaTeX file prepared by the author.